Stepwise recovery of magnesium from low-grade ludwigite ore based on innovative and clean technological route

Xiao-jiao FU, Man-sheng CHU, Li-hua GAO, Zheng-gen LIU

School of Metallurgy, Northeastern University, Shenyang 110819, China

Abstract: A novel and clean technological route for the comprehensive utilization of low-grade ludwigite ore was proposed, in which magnesium was extracted by metallizing reduction−magnetic separation, sulfuric acid leaching and ethanol precipitation operation. Meanwhile, iron-rich product, silicon-rich product and boron-rich product were obtained, respectively. In the process of metallizing reduction−magnetic separation, 94.6% of magnesium was enriched in the non-magnetic substance from the ore reduced at 1250 °C for 60 min with the ore size of 0.50−2.00 mm and coal size of 0.50−1.50 mm. When the non-magnetic substance was leached at 90 °C for 15 min with the liquid-to-solid ratio of 7:1, 87.4% of magnesium was leached into the liquor separated from silicon gathering in leaching residue. The ethanol precipitation was conducted for 30 min with the ethanol-to-original liquid volume ratio of 1.5:1 at room temperature. 97.2% of magnesium was precipitated out with the initial concentration of 0.8 mol/L in the form of $MgSO_4 \cdot 7H_2O$.

Key words: ludwigite; magnesium; metallizing reduction; leaching; precipitation; recovery

1 Introduction

The boron resources in China, ranking forth next to Turkey, the USA and Russia, have low quality containing 8.4% B_2O_3 on average. Chinese boron ores mainly include ascharite, ludwigite and salt lake boron ore [1−3]. With the high demand of boron resources, ascharite is running out. Due to the poor geographic location, transportation condition and exploration condition, salt lake boron ore in Qing-Tibet Plateau cannot be mined at a large scale by now. Ludwigite in northeastern China has become the available resource with great potential [4−7]. Unfortunately, there is no mature industrial process for the comprehensive utilization of ludwigite due to its complex mineralogy, fine mineral dissemination and difficult components separation. Especially, the low grade ores are usually discarded as waste, leading to the farmland occupation, environment pollution and resource wasting.

In traditional treatment process, ludwigite original ore was ground and separated from gangue minerals via magnetic−gravitational dress process to obtain boron-bearing iron concentrate and boron concentrate. The concentrates were treated through pyrometallurgical or hydrometallurgical processes to produce qualitative materials for the corresponding industries. About 85%−90% of iron can be gathered in the iron concentrate and 70%−73% of boron can be gathered in the boron concentrate, but most of magnesium and silicon were discharged in tailings. In addition, traditional separation methods are unsuitable for multi-phase and complex ores [8−10]. In the pyrometallurgical processes, the iron concentrate was pelletized and smelted in blast furnace to produce the boron-bearing pig iron and boron-rich slag. But problems exist in this process limiting industrial application, such as low capacity, high coke ratio, severe brasque erosion and low activity of the boron-rich slag [11−15]. Iron concentrate can be treated by non-blast furnace process: bulks or pellets were reduced utilizing non-coke coal or reducing gas in furnace, and reduced products were separated via melting separation or magnetic separation to produce the qualitative iron materials and boron-rich slag. Non-blast furnace process is a good practice to deal with complex ores, but it is not commonly used for original ore [16−23].

Corresponding author: Man-sheng CHU; Tel: +86-24-83684959; E-mail: chums@neu.edu.cn

Boron concentrate or boron-rich slag was leached with acid or base to get boric acid or borax. Limited by technology capability, only high grade original ore with B_2O_3 content higher than 12% can be dealt with hydrometallurgical processes. Low grade ludwigite ores are abandoned as waste causing vicious circle for environment pollution [24−27]. The coal-based direct reduction utilizing sodium carbonate was another attempt for the extraction of boron and iron from ludwigite ore. Alkali-activation of boron and metallization of iron were synchronously achieved during carbothermic reduction of ludwigite ore in the process of sodium carbonate. Consequently, boron was extracted in the form of sodium metaborate with water at room temperature during ball mill grinding, and metallic iron powder was recovered from the leaching−filtering residue by magnetic separation [28−30].

In this work, an integrated technological route was proposed for the comprehensive utilization of low-grade ludwigite original ore as shown in Fig. 1. Throughout the new process, the main valuable components, including iron, boron, magnesium and silicon can be separated stepwise. The obtained products can be used for the corresponding industries, making the initially hazardous material be a valuable resource. The details of magnesium recovery were mainly researched in the process. A total magnesium recovery of 80.3% was achieved under the optimized conditions.

2 Experimental

2.1 Materials

The chemical compositions of ludwigite ore from Dandong region in China are listed in Table 1. The sample contained 30.7% TFe, 8.6% B_2O_3, 26.4% MgO and 14.3% SiO_2. The XRD analysis of the material is shown in Fig. 2. The main phases of ludwigite ore included magnetite, serpentine, ludwigite, szajbelyite, magnesioferrite and periclase. The non-coking coal with fixed carbon content of 59.3% was served as the reductant in the metallizing reduction process. Concentrated sulfuric acid was used in the non-magnetic leaching process. The analytical reagents and deionized water were used in the experiment.

2.2 Theories and methods

As depicted in Fig. 1, the experiment mainly included: (1) metallizing reduction−magnetic separation of ludwigite ore for Fe enrichment in the magnetic substance, and separation of magnetic substance from Mg-rich non-magnetic substance; (2) sulfuric acid leaching of the non-magnetic substance for Si enrichment in leaching residue, and Mg and B extraction in leaching liquor; (3) ethanol precipitation of Mg and boron-rich materials isolation. Details of treatment steps were described as follows.

2.2.1 Metallizing reduction−magnetic separation of ludwigite ore

When solid carbon exists, the reduction reactions of iron oxides and magnesium oxides in ludwigite ore may take place as described in Equations (1)−(7). Additionally, CO_2 generating in the system can participate in the Boudouard reaction to form CO. Therefore, the metal oxides may react with CO in term of gas−solid reaction as shown in Equations (8)−(14). The expressions of $\Delta G^{\ominus}$ are shown in Table 2. Within the temperature range of 0−1500 °C, iron oxides can be reduced to metal iron by C or CO, while neither metal magnesium nor carbides can be formed. By controlling the reduction conditions, the iron particles nucleation, aggregation and growth can be improved, and iron separation from magnesium and other elements is promoted.

Prior to the reduction process, the ludwigite ore and coal were crushed and screened at certain particle sizes separately. Then, the ludwigite ore was mixed with a certain ratio of coal (the coal mass was about 20% of ore). The uniform mixture of the materials was added into a graphite crucible, put into high temperature furnace and reduced under the preset temperature for a period of time. After reduction, the reduced samples
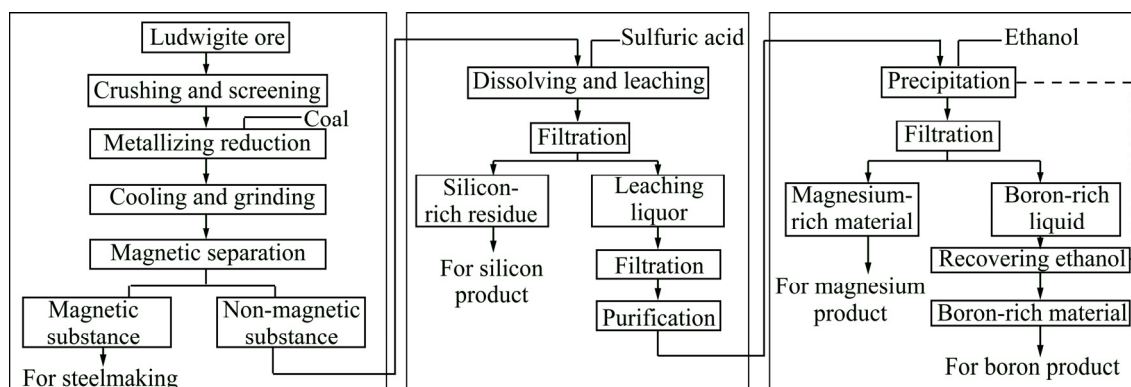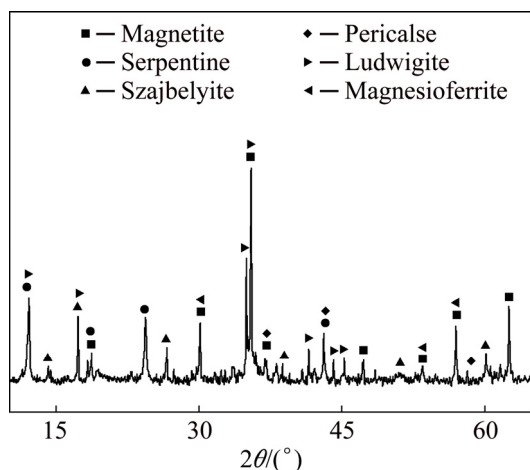

Fig. 1 Integrated technological route for comprehensive utilization of low-grade ludwigite ore

Table 1 Chemical compositions of ludwigite ore used in this study (mass fraction, %)

TFe	FeO	Fe_2O_3	B_2O_3	MgO	SiO_2	CaO	Al_2O_3
30.7	17.6	24.3	8.6	26.4	14.3	0.2	0.9

Fig. 2 XRD pattern of ludwigite ore

Table 2 Possible reactions of iron oxides or magnesium oxides with C and CO

Equation No.	Reaction	$\Delta G^{\Theta}/(\text{ kJ·mol}^{-1})$
(1)	$3Fe_2O_3(s)+C(s)= 2Fe_3O_4(s)+CO(g)$	$72.1614-0.2258T$
(2)	$Fe_3O_4(s)+C(s)= 3FeO(s)+CO(g)$	$142.7147-0.2045T$
(3)	$1/4Fe_3O_4(s)+C(s)= 3/4Fe(s)+CO(g)$	$118.2950-0.1646T$
(4)	$FeO(s)+C(s)= Fe(s)+CO(g)$	$110.1551-0.1513T$
(5)	$MgO(s)+C(s)= Mg(g)+CO(g)$	$445.2943-0.2182T$
(6)	$1/3MgO(s)+C(s)= 1/3MgC_2(s)+1/3CO(g)$	$174.0779-0.0718T$
(7)	$2/5MgO(s)+C(s)= 1/5Mg_2C_3(s)+2/5CO(g)$	$189.5337-0.0839T$
(8)	$3Fe_2O_3(s)+CO(g)= 2Fe_3O_4(s)+CO_2(g)$	$-51.2745-0.0511T$
(9)	$Fe_3O_4(s)+CO(g)= 3FeO(s)+CO_2(g)$	$19.2787-0.0298T$
(10)	$1/4Fe_3O_4(s)+CO(g)= 3/4Fe(s)+CO_2(g)$	$-5.1411+0.01009T$
(11)	$FeO(s)+CO(g)= Fe(s)+CO_2(g)$	$-13.2010+0.0234T$
(12)	$MgO(s)+CO(g)= Mg(g)+CO_2(g)$	$318.7589-0.0341T$
(13)	$1/5MgO(s)+CO(g)= 1/5MgC_2(s)+3/5CO_2(g)$	$30.3851+0.0618T$
(14)	$1/4MgO(s)+CO(g)= 1/8Mg_2C_3(s)+5/8CO_2(g)$	$41.3110+0.0568T$

were cooled to room temperature in the crucible isolated from the atmospheric environment. The reduced samples were ground to less than 0.074 mm (>80% in mass), and then separated by a DTCXG-ZN50 magnetic tube under the magnetic field intensity of 50 mT. Metallic iron was enriched in the obtained magnetic substance, and the non-magnetic substance including Mg, Si and B was subjected to the acid leaching process subsequently. The recovery rate of Fe in the magnetic substance and the recovery rate of Mg in the non-magnetic substance were calculated according to Equations (15) and (16), respectively:

$$\eta(\text{Fe})_m=[w(\text{TFe})_m \times m_m]/[w(\text{TFe})_s \times m_s] \times 100\% \quad (15)$$

$$\eta(\text{Mg})_n=[w(\text{MgO})_n \times m_n]/[w(\text{MgO})_s \times m_s] \times 100\% \quad (16)$$

where $\eta(\text{Fe})_m$ is the recovery rate of Fe in magnetic substance, %; $w(\text{TFe})_m$ is the mass fraction of total Fe in magnetic substance, %; m_m is the mass of magnetic substance, g; $w(\text{TFe})_s$ is the mass fraction of total Fe in reduced sample subjected to magnetic separation, %; m_s is the mass of reduced sample subjected to magnetic separation, g; $\eta(\text{Mg})_n$ is the recovery rate of Mg in non-magnetic substance, %; $w(\text{MgO})_n$ is the mass fraction of MgO in non-magnetic substance, %; m_n is the mass of non-magnetic substance, g; $w(\text{MgO})_s$ is the mass fraction of MgO in reduced sample subjected to magnetic separation, %.

2.2.2 Sulfuric acid leaching of non-magnetic substance

After the metallizing reduction−magnetic separation, magnesium mainly gathered in the non-magnetic substance in terms of suanite and forsterite, and the ionic equations of the reactions between the two phases with sulfuric acid are shown as Equations (17) and (18):

$$Mg_2B_2O_5+4H^++H_2O=2Mg^{2+}+2H_3BO_3 \quad (17)$$
$$Mg_2SiO_4+4H^+=2Mg^{2+}+SiO_2+2H_2O \quad (18)$$
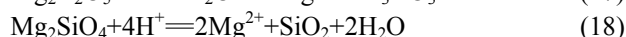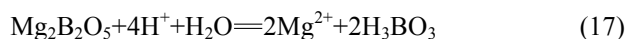
Based on the general principles of chemical reactions, there is

$$\Delta G_T^{\Theta} = \sum_i v_i \cdot \Delta G_{f,T,i}^{\Theta} \quad (19)$$

$$\lg K_T^{\Theta} = -\Delta G_T^{\Theta} / (2.303RT) \quad (20)$$

When the reaction reaches equilibrium state, $\Delta G_T=0$, there is,

$$\Delta G_T^{\Theta} = -RT \ln Q_{eq} = -RT \ln K_T^{\Theta} = -2.303RT \lg K_T^{\Theta} \quad (21)$$

Based on the isothermal equation of van't Hoff,

$$\Delta G_T = \Delta G_T^{\Theta} + RT \ln Q_T =$$
$$-2.303RT \lg K_T^{\Theta} + 2.303RT \lg Q_T =$$
$$-2.303RT \lg(K_T^{\Theta}/Q_T) \quad (22)$$

where v_i is the stoichiometric coefficient, "−" for reactant, "+" for product; R is the mole gas constant; T is

the thermodynamic temperature; Q_T is the reaction quotient at T; ΔG_T^{Θ} is the standard Gibbs free energy of the reaction at T; $\Delta G_{f,T,i}^{\Theta}$ is the standard Gibbs free energy of the reactant or the product at T; K_T^{Θ} is the standard equilibrium constant of the reaction at T.

The software FactSage was used for the thermodynamic calculation of the above reactions, and the results are shown in Table 3. When the temperature changes from 25 to 100 °C, the ΔG_T^{Θ} of Equations (17) and (18) increase and are still much less than zero; the K_T^{Θ} calculated based on Equation (20) are all higher than 10^{20}. Thermodynamically, the above two reactions can advance completely. The expressions of Q_T for the two reactions are shown as Equations (23) and (24), respectively:

$$Q_T = (c(Mg^{2+})/c^{\Theta})^2/(c(H^+)/c^{\Theta})^4 \tag{23}$$

$$Q_T = (c(Mg^{2+})/c^{\Theta})^2/(c(H^+)/c^{\Theta})^4 \tag{24}$$

where $c(Mg^{2+})$ is the mole concentration of Mg^{2+}, mol/L; $c(H^+)$ is the mole concentration of H^+, mol/L; c^{Θ} is the standard concentration, mol/L. The value of pH in the leaching system is controlled below 2, in which the $c(H^+)$ is 10^{-2} mol/L. At 100 °C, if Q_T is equals to K_T^{Θ}, the equilibrium mole concentration of Mg^{2+} must above 1.84×10^6 mol/L, which is impossible even if all of magnesium in the non-substance is leached out. Theoretically, suanite and forsterite can react with sulfuric acid completely, while magnesium and boron will be leached into the liquor, and silicon will be gathered in the residue.

The non-magnetic substance obtained from the magnetic separation process was leached with sulfuric acid (the acid dosage was 85%). The non-magnetic substance and deionized water with a certain liquid-to-solid ratio were added into a three-necked flask. The flask installed with reflux device and stirring device (stirring speed maintaining constantly at 400 r/min) was placed in the electric-heated thermostatic water bath. After being heated to the set temperature, the sulfuric acid was injected into the flask with stirring. At the beginning 10% of acid was injected slowly to avoid splash, then the remaining acid was injected as quickly as possible. After leaching, the solution was filtered to separate dissolved Mg, B from Si which was enriched in the leaching residue. The leaching liquor was collected for the subsequent precipitation process to separate Mg from B. The leaching rate of Mg in this period was calculated according to Equation (25):

$$\eta(Mg)_l=[w(MgO)_n\times m_n-w(MgO)_r\times m_r]/$$
$$[w(MgO)_n\times m_n]\times100\% \tag{25}$$

where $\eta(Mg)_l$ is the leaching rate of Mg in acid leaching process, %; $w(MgO)_r$ is the mass fraction of MgO in leaching residue, %; m_r is the mass of leaching residue, g.

2.2.3 Ethanol injection and precipitation of leaching liquor

After sulfuric acid leaching and filtration, magnesium and boron were concentrated in the liquor, and silicon was gathered in the residue. Besides, a little amount of iron remaining in the non-magnetic substance also existed in the liquor. Trace impurities such as calcium and aluminum also can react with sulfuric acid, and the product can either gather in the residue as a poorly soluble compound(like $CaSO_4$), or enter into the liquor(like $Al_2(SO_4)_3$). Fe^{2+} and Al^{3+} were the main impurities in the leaching liquor, and the suitable removal operation can be set out based on the $\varphi-pH$ diagram of the $Mg-Fe-Al-H_2O$ system drawn by the software FactSage as Fig. 3. The phase compositions of each region are presented in Table 4. As can be seen, in the stable region of water, different ions can be hydrolytically precipitated through controlling the electric potential and pH of the liquor to achieve the impurities removal. At relatively low pH, Fe^{2+} needs to be oxidized as only Fe^{3+} can be hydrolytically precipitated completely. During this process, Mg^{2+} should not be precipitated to avoid target element loss. While under relatively high pH, Al^{3+} can dissolve in term of AlO_2^- in the basic liquor. Therefore, reasonable conditions should be selected to remove aluminum impurity.

Table 3 Thermodynamic parameters of reaction between suanite and forsterite with sulfuric acid

T/K	Reaction (17)			Reaction (18)		
	ΔG_T^{Θ}/(kJ/mol)	ΔK_T^{Θ}	$c(Mg^{2+})_{eq}$/(mol·L^{-1})	ΔG_T^{Θ}/(kJ/mol)	ΔK_T^{Θ}	$c(Mg^{2+})_{eq}$/(mol·L^{-1})
298.15	−160.42	1.27×10^{28}	1.13×10^{10}	−181.92	7.44×10^{31}	8.62×10^{11}
313.15	−157.86	2.15×10^{26}	1.46×10^{9}	−179.15	7.63×10^{29}	8.73×10^{10}
333.15	−154.31	1.56×10^{24}	1.24×10^{8}	−175.63	3.44×10^{27}	5.87×10^{9}
353.15	−150.58	1.87×10^{22}	1.37×10^{7}	−172.29	3.04×10^{25}	5.52×10^{8}
373.15	−146.66	3.39×10^{20}	1.84×10^{6}	−169.11	4.70×10^{23}	6.86×10^{7}
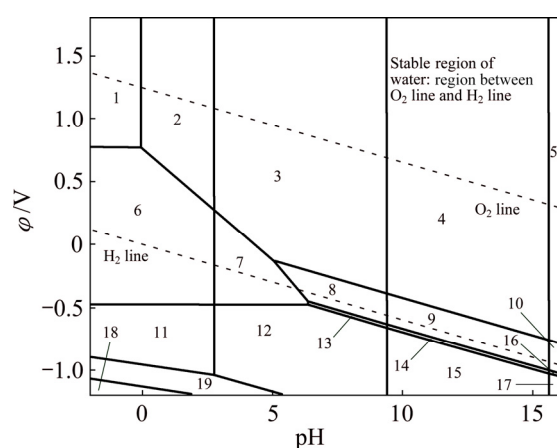
Fig. 3 φ−pH diagram of Mg−Fe−Al−H_2O system (T=298.15 K, c_{total}=0.01 mol/L, $c(Fe^{2+})$ =0.0004 mol/L, $c(Al^{3+})$=0.0004 mol/L)

As shown in Fig. 3, in the stable region of water, in the Regions 3 and 8 the iron and aluminum are precipitated while magnesium is still in the liquor as ionic state. The corresponding phase compositions are $Fe_2O_3+Al_2O_3(H_2O)+Mg^{2+}$ and $Fe_3O_4+Al_2O_3(H_2O)+Mg^{2+}$. In order to reduce the operation difficulty, iron should be oxidized to Fe^{3+} to expand the pH range in the impurities removal process. Most iron in the non-magnetic substance is ferrous or metallic iron after metallizing reduction−separation process, suitable oxidant should be injected at the same time to avoid including other impurities. Based on the above analyses, the suitable removal operation in this study was to inject hydrogen peroxide for Fe^{2+} oxidation to achieve 105% oxidation of Fe^{2+} to Fe^{3+} in the non-magnetic substance. Then, MgO

was injected to adjust the pH of the liquor at 4−6 to avoid bringing out other impurities. The purified liquor without iron and aluminum was obtained after filtration.

Judging from the Born−Haber circle in the dissolving process, factors that determine the dissolving capacity of the ionic crystal are mainly the solvation energy of ion, the lattice energy of ionic crystal, and the entropy of dissolving process. The relationship expressions of these factors are as Equations (26) and (27):

$$\Delta G_S=\Delta H_S-T\Delta S_S \qquad (26)$$

$$\Delta H_S=U+\Delta H(+)+\Delta H(-) \qquad (27)$$

where ΔG_S is the Gibbs free energy of dissolving process; ΔH_S is the enthalpy of dissolving process; ΔS_S is the entropy of dissolving process; U is the crystal lattice of ionic crystal; $\Delta H(+)$ is the solvation energy of positive ion; $\Delta H(-)$ is the solvation energy of negative ion.

The thermodynamic data of magnesium sulfate in different solvent systems are shown in Table 5. The solvation energy of Mg^{2+} in water−ethanol system is quite different from that in water system, and ΔG_S in water−ethanol system is much higher than zero, which means that magnesium sulfate is hard to dissolve in this system [31]. Besides, according to the theory that similarities can be solvable easily in each other, boron acid can dissolve in the system [32]. Therefore, the operation of injecting ethanol into the liquor to separate magnesium from boron is feasible. Compared with the traditional method of high temperature magnesium sulfate crystallization, its energy consumption is lower and operation is simpler.

Table 4 Corresponding phases in Fig. 3

Region	Phase	Region	Phase
1	$Fe^{3+}+Al^{3+}+Mg^{2+}$	11	$Fe+Al^{3+}+Mg^{2+}$
2	$Fe_2O_3+Al^{3+}+Mg^{2+}$	12	$Fe+Al_2O_3(H_2O)+Mg^{2+}$
3	$Fe_2O_3+Al_2O_3(H_2O)+Mg^{2+}$	13	$Fe(OH)_2+Al_2O_3(H_2O)+Mg^{2+}$
4	$Fe_2O_3+Al_2O_3(H_2O)+Mg(OH)_2$	14	$Fe(OH)_2+Al_2O_3(H_2O)+Mg(OH)_2$
5	$Fe_2O_3+ AlO_2^- +Mg(OH)_2$	15	$Fe+Al_2O_3(H_2O)+Mg(OH)_2$
6	$Fe^{2+}+Al^{3+}+Mg^{2+}$	16	$Fe(OH)_2+ AlO_2^- +Mg(OH)_2$
7	$Fe^{2+}+Al_2O_3(H_2O)+Mg^{2+}$	17	$Fe+ AlO_2^- +Mg(OH)_2$
8	$Fe_3O_4+Al_2O_3(H_2O)+Mg^{2+}$	18	$Fe+AlH_3+Mg^{2+}$
9	$Fe_3O_4+Al_2O_3(H_2O)+Mg(OH)_2$	19	$Fe+AlH_3+MgH_2$
10	$Fe_3O_4+ AlO_2^- +Mg(OH)_2$		

Table 5 Thermodynamic data of magnesium sulfate at 298.15 K (kJ/mol)

Solvent	$\Delta H(+)$	$\Delta H(-)$	U	ΔH_S	$T\Delta S_S$	ΔG_S
Water	−1966.48	−1041.82	2888.37	−119.93	62.47	−182.40
Water−ethanol	−374.96	−1041.82	2888.37	1471.59	166.22	1305.37

After impurity removal and liquid condensation, certain amount of ethanol was added into the leaching liquor and soon white haze appeared in the system. After standing for a period of time, Mg^{2+} ions were precipitated completely and separated from boron by filtration. Mg-rich product was found in the precipitation after putting into a vacuum drying oven at 40 °C for 2 h. Boron-rich material was obtained through ethanol recovery and condensing crystallization. The recovery rate of Mg in this period was calculated according to Equation (28):

$$\eta(Mg)_p=[w(Mg)_p\times m_p]/[c(Mg)_l\times V_1\times M(Mg)]\times100\% \quad (28)$$

where $\eta(Mg)_p$ is the recovery rate of Mg in precipitation, %; $w(Mg)_p$ is the mass fraction of Mg in precipitation, %; m_p is the mass of precipitation, g; $c(Mg)_l$ is the mole concentration of Mg^{2+} in the liquor before ethanol addition, mol/L; V_1 is the volume of the liquor before ethanol addition; $M(Mg)$ is the molar mass of Mg, g/mol.

3 Results and discussion

3.1 Metallizing reduction−magnetic separation for ludwigite ore

Two key problems of metallizing reduction− magnetic separation process were: (1) enhancing the transformation rate of the low/non-magnetic iron oxides in the ore to high-magnetic metallic iron in the reduced sample; (2) promoting the metallic iron particles nucleation, aggregation and growing to larger particles. High metallization rate (the rate of metallic iron content to total iron content in the sample) and large metallic iron particles were beneficial to enriching iron in magnetic substance separated from magnesium, silicon and boron in non-magnetic substance treated with magnetic-separation.

The effects of different factors on the recovery rate of Mg and Fe in this period are shown in Fig. 4. As shown in Fig. 4(a), high temperature had a favorable effect on the elements recovery. With temperature increasing from 1100 to 1250 °C, the recovery rate of Fe in the magnetic substance increased from 72.5% to 88.8%, and the recovery rate of Mg in the non-magnetic substance increased from 87.2% to 95.4%.

As shown in Fig. 4(b), the recovery rate of Fe in the magnetic substance increased significantly as the reduction time increased from 10 to 60 min, while the recovery rate of Mg in the non-magnetic substance maintained the high values around 94%. The reduction temperature and time were two important factors
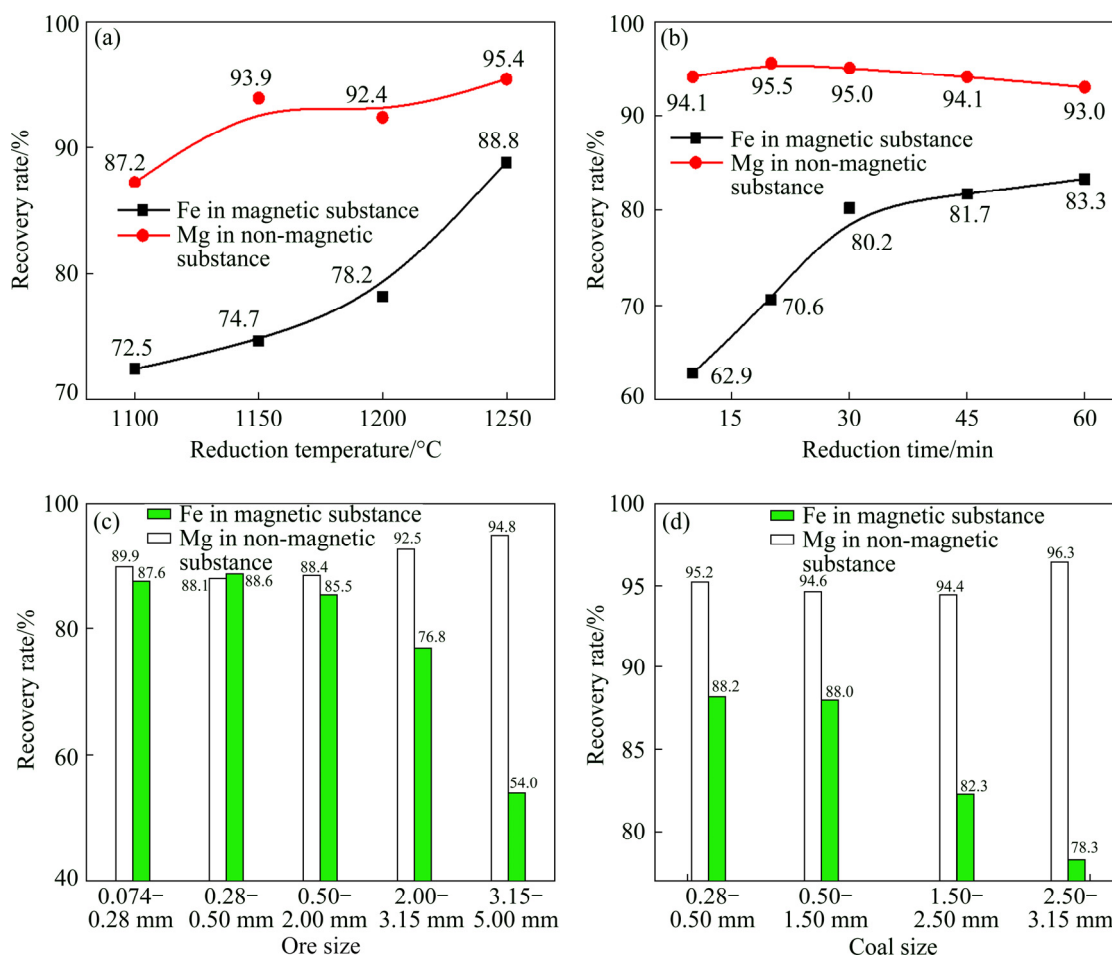

Fig. 4 Results of metallizing reduction−magnetic separation process

influencing the metallization rate and metallic iron particles size in the reduced sample. When the reduction temperature was low and the time was short, the reduction was not sufficient. The metallic iron particles were small, isolated, dispersed and combined with slag phase, which was against magnetic separation. With the increase of the temperature and time, the thermodynamic and kinetic conditions of reduction reactions were improved remarkably, and the nucleation, aggregation and growing of metallic iron particles were further facilitated, which was beneficial to magnetic separation.

As shown in Figs. 4(c) and (d), the ore size and coal size presented the similar trend on the influence of the recovery rates of elements. With the smaller material size, the separation operation was more efficient. This can be explained by the microstructure of the reduced sample in Fig. 5. When the material size was coarse, the contact area of ore and coal was small, which was against oxide reduction and iron particle aggregation. As a result, most iron-bearing unreduced materials entered the non-magnetic substance, leading to the low recovery rate of Fe in the magnetic substance. Meanwhile, the recovery rate of Mg in non-magnetic substance was relatively high. When the material size was finer, the contact area of ore and coal became larger, the metallizing rate increased and the metallic iron particle can be gathered and grown, and this was beneficial to the efficient magnetic separation. Finally, metallic iron was enriched in the magnetic substance with high metallizing rate of 93.5%, which can be used as raw materials for steelmaking industry. Mg was enriched with the recovery rate of 94.6% in the non-magnetic substance whose main phases were forsterite and suanite. The non-magnetic substance was subjected to acid leaching process subsequently. The XRD and SEM analyses of the separation products are shown in Fig. 6.

3.2 Sulfuric acid leaching of non-magnetic substance

Effect of different factors on the sulfuric acid leaching of Mg from the non-magnetic substance was further examined, and the results are shown in Fig. 7. As the leaching temperature increased, the leaching rate of Mg increased obviously. When the temperature was 90 °C, the leaching rate of Mg was 83.3%. The increase of temperature promoted the chemical reaction rate and the diffusion rate. In addition, under lower temperature, the reactant cannot decompose completely, which limited the separation efficiency during the filtration operation. The XRD analyses of leaching residue (Fig. 8) indicated that, when the leaching temperature was low, the main patterns of the leaching residue remained suanite ($Mg_2B_2O_5$) and forsterite (Mg_2SiO_4). The result proved that the low temperature prevented the efficient leaching of Mg and the separation from Si. With the temperature and the leaching reaction degree increasing, the characteristic diffraction peaks of suanite and forsterite wore off. When the temperature was 90 °C, suanite
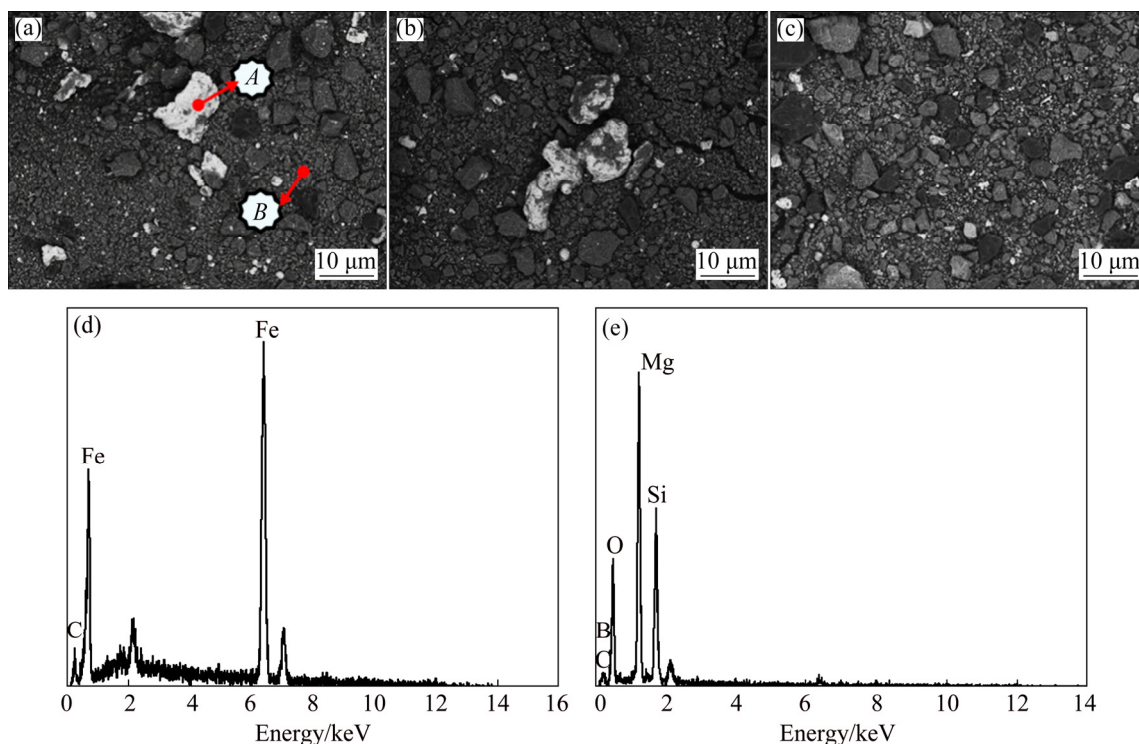

Fig. 5 SEM images (a−c) and EDS analysis results (d, e) of reduced samples with different ore sizes: (a) 0.074−0.28 mm; (b) 0.50−2.00 mm; (c) 2.00−3.15 mm; (d) Area *A*; (e) Area *B*
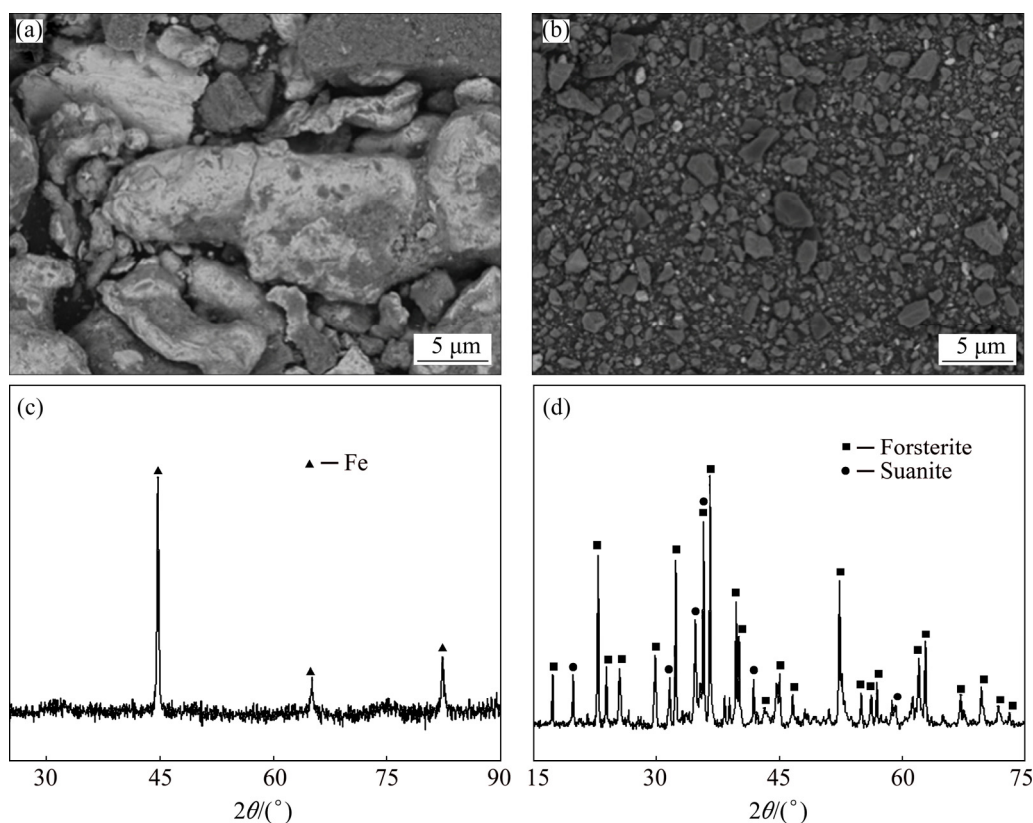
Fig. 6 SEM images (a, b) and XRD patterns (c, d) of separation products: (a, c) Magnetic substance; (b, d) Non-magnetic substance
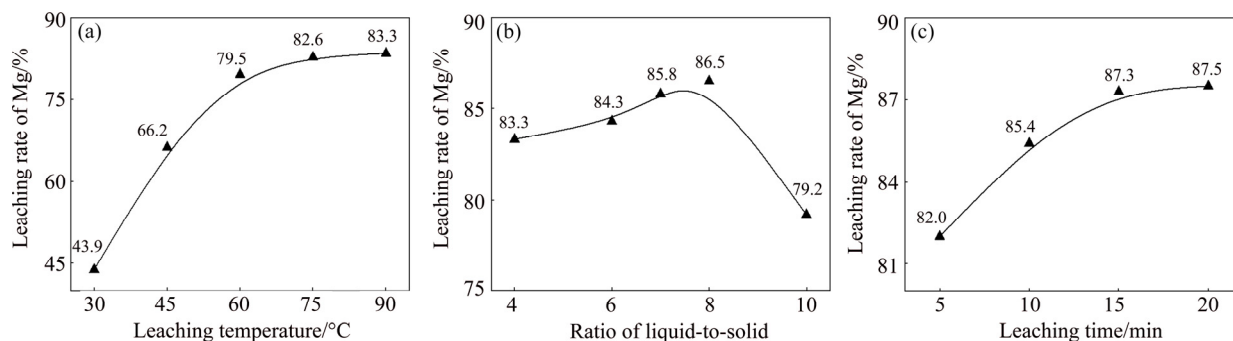

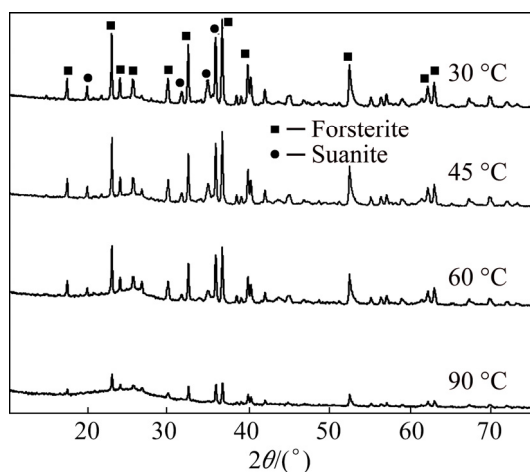**Fig. 7** Results of sulfuric acid leaching of Mg from non-magnetic substance

Fig. 8 XRD patters of leaching residue at different temperatures

almost disappeared and the characteristic diffraction peaks of forsterite weakened evidently. Only a little forsterite existed in the leaching residue, and the leaching rate of Mg was high. In addition, in the leaching residue, there were no distinct characteristic diffraction peaks of crystal SiO_2, whose diffraction peaks values of 2θ were 26.662°, 20.874°, 50.185°, 60.009°, 36.573°, 39.504°. Instead, steamed buns-like peaks appeared in the range of 15°−30°, and this dispersion diffraction curve was identical with the XRD curve of amorphous SiO_2 exactly. This indicated that SiO_2 generated from the reaction of forsterite and sulfuric acid was mainly in amorphous state, which had strong water absorbing capacity. Thus the increase of the lixivium viscosity had negative influence on the filtration operation.

As shown in Fig. 7(b), when the ratio of liquid-to-solid was lower than 7, the leaching rate of Mg increased gradually with the increase of the ratio. The increase of the ratio of liquid-to-solid improved the fluidity of the lixivium for the leaching reaction process, leading to higher Mg leaching rate. When the ratio of liquid-to-solid increased higher than 8, the leaching rate of Mg showed a declining tendency. With the higher ratio of liquid-to-solid, the sulfuric acid concentration was diluted. Under the circumstances, the acid concentration played a dominant role in the leaching process, and the Mg leaching rate decreased. Meanwhile, the amorphous SiO_2 generated in the process affected the efficiency of the filtration operation. Therefore, the suitable ratio of liquid-to-solid in the leaching process was about 7:1−8:1. As shown in Fig. 7(c), with the extension of the leaching time, the leaching rate of Mg increased gradually. When the leaching time was 15 min, the leaching rate of Mg reached 87.4%. If the time increased to 20 min, the leaching rate changed a little.

Additionally, the increase of leaching time led to the increase of impurity concentration, amorphous SiO_2 water absorption, and lixivium viscosity, which reduced filtration operation efficiency. Therefore, the suitable leaching time was 15−20 min.

The SEM and EDS-mapping images of the non-magnetic substance and the leaching residue are shown in Fig. 9. Most of the particles in the non-magnetic substance appeared to be lump with smooth surface. Compared with Fig. 9(a), Fig. 9(d) indicated that irregular holes formed on the surface of the leaching residue, and the particles became smaller. In addition, the distribution density of Mg in the residue was significantly lower than that before the leaching operation. Meanwhile, the element Si tended to be enriched in the leaching residue and it can be used as raw materials for silicon recovery. After purification and concentration, the leaching liquor was collected for subsequent precipitation process to separate Mg from B.
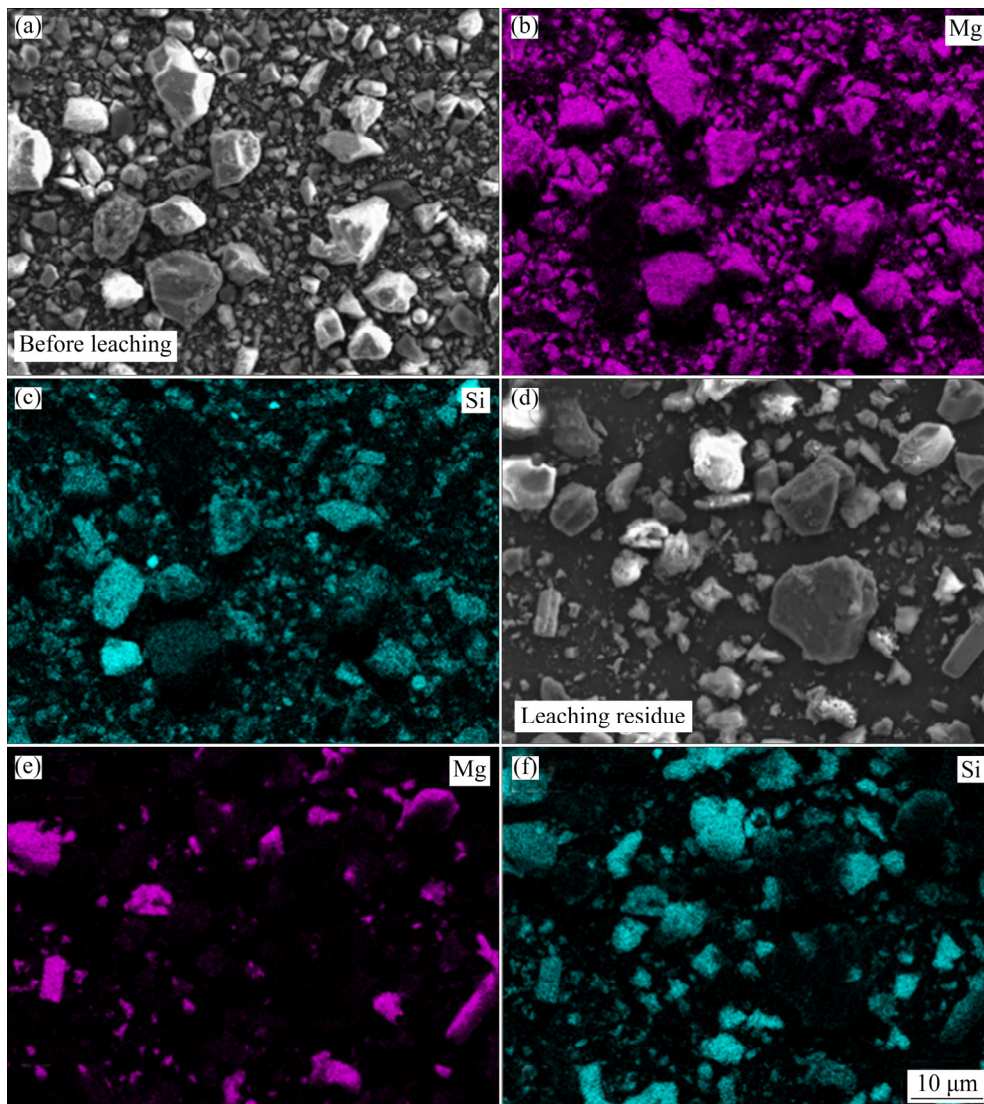

Fig. 9 SEM and EDS-mapping images of non-magnetic substance (a, b, c) and leaching residue (d, e, f)

3.3 Recovery of Mg from leaching liquor by adding ethanol

Effects of different factors on the recovery rate of Mg from the composite system are shown in Fig. 10. As shown in Fig. 10(a), with more ethanol adding into the leaching liquor, the recovery rate of Mg increased. When the volume ratio of ethanol-to-original liquid was 1.5:1, the recovery rate of Mg reached 94.8%. As shown in Fig. 10(b), when the time was 30 min, the recovery rate was 97.2%. The precipitation of Mg stayed basically constant with the increase of time. As shown in Fig. 10(c), $MgSO_4$
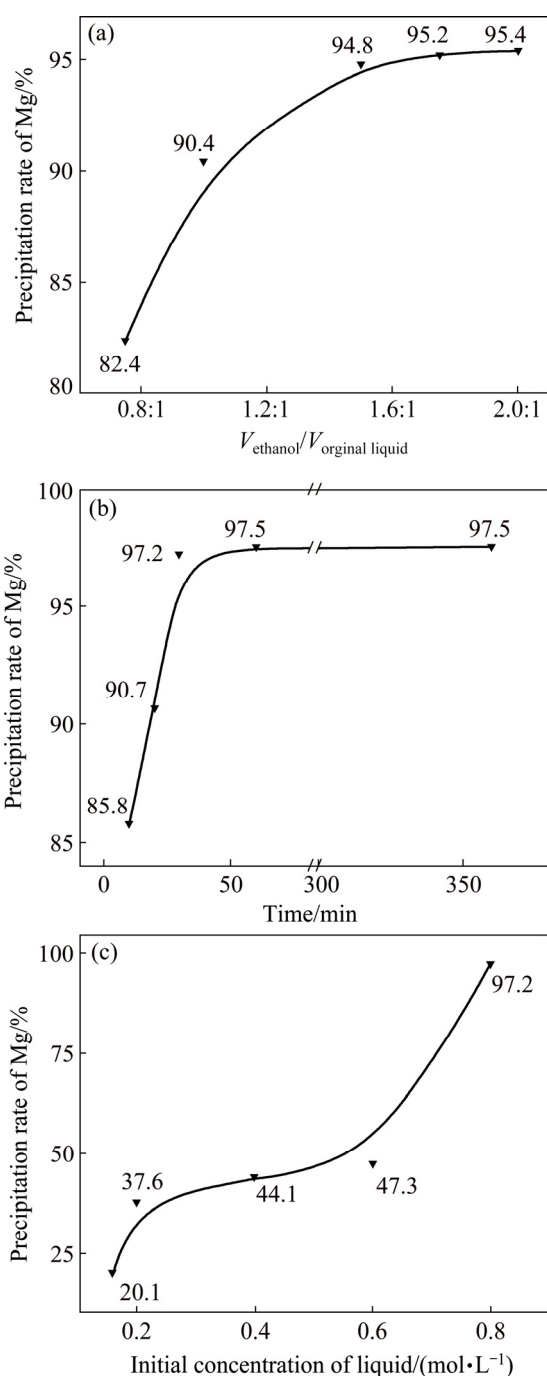
can be precipitated at a relatively low initial concentration (0.8 mol/L) in the water−ethanol composite system, which was much lower than the saturation concentration (1.83−3.23 mol/L) of $MgSO_4$ in aqueous solution at room temperature range.

Therefore, the precipitation process with water−ethanol composite system had the advantages of minimum requirement of liquor concentration and operation temperature, while the ethanol can be recycled in the process. The product of the precipitation was $MgSO_4·7H_2O$, which was proved by the XRD analysis in Fig. 11. The residue liquor was collected for ethanol recovery followed by boron extraction to obtain boron-rich material.
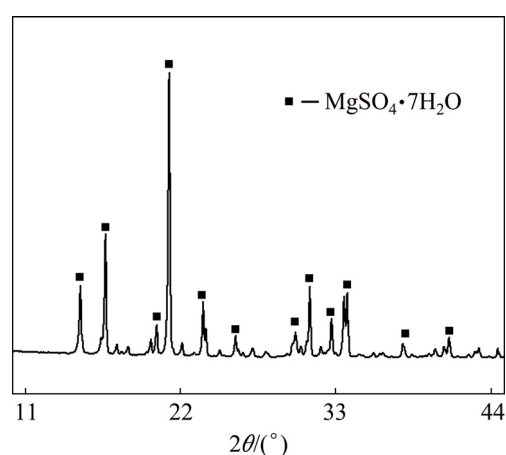

Fig. 11 XRD pattern of bearing-Mg precipitation

4 Conclusions

1) In the process of metallizing reduction−magnetic separation, 94.6% of magnesium was enriched in the non-magnetic substance from the ore reduced at 1250 °C for 60 min with the ore size of 0.50−2.00 mm and coal size of 0.50−1.50 mm. Meanwhile, iron-rich magnetic substance was obtained for steel making. The technological parameters mainly affected the metallization rate and metallic iron particle size, which determined the separation efficiency.

2) When the non-magnetic substance was leached at 90 °C for 15 min with the ratio of liquid-to-solid 7:1, 87.4% of magnesium was leached into the liquor separated from silicon gathering in leaching residue. Amorphous SiO_2 generated in the process had a negative influence on the filtration separation efficiency.

3) The ethanol precipitation was conducted for 30 min with the ethanol-to-original liquid volume ratio of 1.5:1 at room temperature and 97.2% of magnesium can be precipitated out with the initial concentration of 0.8 mol/L. The product was $MgSO_4·7H_2O$. The residue liquor was collected for ethanol recovery followed by boron extraction to obtain boron-rich material.

Fig. 10 Effects of different factors on precipitation rate of Mg from composite system

References

[1] YAN Xue-long, CHEN Bin. Chemical and boron isotopic compositions of tourmaline from the Paleoproterozoic Houxianyu borate deposit, NE China: Implications for the origin of borate deposit [J]. Journal of Asian Earth Sciences, 2014, 94: 252−266.

[2] AN Jing, XUE Xiang-xin. Life cycle environmental impact assessment of borax and boric acid production in China [J]. Journal of Cleaner Production, 2014, 66: 121−127.

[3] YU Pei-feng, YANG Xi-yun, XU Hui, SHI Xi-chang, CHEN Ya, YAN Guo-chun. Separation technique for boron and magnesium from salt lake brine and preparation of high-purity magnesium oxide [J]. The Chinese Journal of Nonferrous Metals, 2013, 23(2): 568−576. (in Chinese)

[4] PENG Qi-ming, PALMER M R. The paleoproterozoic Mg and Mg−Fe borate deposits of Liaoning and Jilin provinces, Northeast China [J]. Economic Geology, 2002, 97(1): 93−108.

[5] PENG Qi-ming, PALMER M R. The paleoproterozoic boron deposits in eastern Liaoning, China: A metamorphosed evapotire [J]. Precambrian Research, 1995, 72(3−4): 185−197.

[6] LU Yuan-fa, CHENG Yu-chuan, LI Hua-qing, XUE Chun-ji, CHENG Fu-wen. Metallogenic chronology of boron deposits in the Eastern Liaoning Paleoproterozoic Rift Zone [J]. Acta Geologica Sinica (English edition), 2005, 79(3): 414−425.

[7] ZHANG Ran, XIE Ying-ming, SONG Jian-feng, XING Li-xin, KONG Ding-feng, LI Xue-mei, HE Tao. Extraction of boron from salt lake brine using 2-ethylhexanol [J]. Hydrometallurgy, 2016, 160: 129−136.

[8] LI Zhi-hang, HAN Yue-xin, LI Yan-jun, GAO Peng. Mechanism of agglomeration and dispersion during flotation process of serpentine and ascharite [J]. The Chinese Journal of Nonferrous Metals, 2014, 24(11): 613−620. (in Chinese)

[9] ZHENG Xue-jia. Boron iron ore processing [M]. Beijing: Chemical Industry Press, 2009. (in Chinese)

[10] LI Zhi-hang, HAN Yue-xin, LI Yan-jun, GAO Peng. Effect of serpentine and sodium hexametaphosphate on ascharite flotation [J]. Transactions of Nonferrous Metals Society of China, 2017, 27(8): 1841−1848.

[11] LIU Su-lan, CUI Chuan-meng, ZHANG Xian-peng. Pyrometallurgical separation of boron from iron in ludwigite ore [J]. ISIJ International, 1998, 38(10): 1077−1079.

[12] YANG Zhong-dong, LIU Su-lan, LI Zhe-fu, XUE Xiang-xin. Oxidation of silicon and boron in boron containing molten iron [J]. Journal of Iron and Steel Research, International, 2007, 14(6): 32−36.

[13] SUI Zhi-tong, ZHANG Pei-xin, YAMAUCHI C. Precipitation selectivity of boron compounds from slags [J]. Acta Materialia, 1999, 47(4): 1337−1344.

[14] JIANG Tao, XUE Xiang-xin. Synthesis of (Ca, Mg) -α'-Sialon-AlN-BN powders from boron-rich blast furnace slag by microwave carbothermal reduction-nitridation [J]. Transactions of Nonferrous Metals Society of China, 2012, 22(12): 2984−2990.

[15] JIANG Tao, WU Jun-bin, XUE Xiang-xin, DUAN Pei-ning, CHU Man-sheng. Carbothermal formation and microstructural evolution of α'-Sialon-AlN-BN powders from boron-rich blast furnace slag [J]. Advanced Powder Technology, 2012, 23: 406−413.

[16] LI Yong-li, QU Jing-kui, WEI Guang-ye, QI Tao. Influence of Na_2CO_3 as additive on direct reduction of boron-bearing magnetite concentrate [J]. Journal of Iron and Steel Research, International, 2016, 23(2): 103−108.

[17] DING Yin-gui, WANG Jing-song, WANG Guang, MA Sai, XUE Qing-guo. Comprehensive utilization of paigeite ore using iron nugget making process [J]. Journal of Iron and Steel Research, International, 2012, 19(6): 9−13.

[18] YU Jian-wen, HAN Yue-xin, GAO Peng, LI Yan-jun. Recovery of boron from high-boron iron concentrate using reduction roasting and magnetic separation [J]. Journal of Iron and Steel Research, International, 2017, 24(2): 131−137.

[19] FU Xiao-jiao, YU Hong-xiang, LIU Zheng-gen, CHU Man-sheng. Experimental study on new process for selective reduction and separation of boron-bearing iron concentrate [J]. Journal of Northeastern University (Natural Science), 2013, 34(7): 966−970. (in Chinese)

[20] YU Jian-wen, HAN Yue-xin, GAO Peng. Thermodynamic behavior of boron minerals in iron concentrate during direct reduction [J]. The Chinese Journal of Nonferrous Metals, 2015, 25(7): 1966−1977. (in Chinese)

[21] WANG Guang, WANG Jing-song, DING Yin-gui, MA Sai, XUE Qing-guo. New separation method of boron and iron from ludwigite based on carbon bearing pellet reduction and melting technology [J]. ISIJ International, 2012, 52(1): 45−51.

[22] FU Xiao-jiao, ZHAO Jia-qi, CHEN Shuang-yin, LIU Zheng-gen, GUO Tong-lai, CHU Man-sheng. Comprehensive utilization of ludwigite ore based on metallizing reduction and magnetic separation [J]. Journal of Iron and Steel Research, International, 2015, 22(8): 672−680.

[23] WANG Guang, XUE Qing-guo, WANG Jing-song. Volume shrinkage of ludwigite/coal composite pellet during isothermal and non-isothermal reduction [J]. Thermochimica Acta, 2015, 621: 90−98.

[24] JIANG Tao, ZHANG Qiao-yi, LIU Ya-jin, XUE Xiang-xin, DUAN Pei-ning. Influence of microwave irradiation on boron concentrate activation with an emphasis on surface properties [J]. Applied Surface Science, 2016, 385: 88−98.

[25] LI Jie, FAN Zhan-guo, LIU Yan-li, LIU Su-lan, JIANG Tao, XI Zheng-ping. Preparation of boric acid from low-grade ascharite and recovery of magnesium sulfate [J]. Transaction of Nonferrous Metals Society of China, 2010, 20(6): 1161−1165.

[26] LI Jie, GUO Xue-dong, GUANG Ming, JIANG Tao. Preparation of boric acid and magnesium sulfate monohydrate from boron-rich slag by sulfuric acid leaching method [J]. The Chinese Journal of Nonferrous Metals, 2014, 24(11): 2943−2950. (in Chinese)

[27] ACARKAN N, BULUT G, KANGAL O, ONAL G. A new process for upgrading boron content and recovery of borax concentrate [J]. Minerals Engineering, 2005, 18(7): 739−741.

[28] LIANG Bin-jun, LI Guang-hui, RAO Ming-jun, PENG Zhi-wei, ZHANG Yuan-bo, JIANG Tao. Water leaching of boron form soda-ash-activated ludwigite ore [J]. Hydrometallurgy, 2017, 167: 101−106.

[29] LI Guang-hui, LIANG Bin-jun, RAO Ming-jun, ZHANG Yuan-bo, JIANG Tao. An innovative process for extracting boron and simultaneous recovering metallic iron from ludwigite ore [J]. Minerals Engineering, 2014, 56: 57−60.

[30] WANG Guang, XUE Qing-guo, WANG Jing-song. Effect of Na_2CO_3 on reduction and melting separation of ludwigite/coal composite pellet and property of boron-rich slag [J]. Transactions of Nonferrous Metals Society of China, 2016, 26(1): 282−293.

[31] HU Qing-fu. Production and utilization of magnesium compounds [M]. Beijing: Chemical Industry Press, 2004. (in Chinese)

[32] ZHENG Xue-jia. A handbook of boron compounds [M]. Beijing: Chemical Industry Press, 2010. (in Chinese)

低品位硼镁铁共生矿中镁资源逐级提取富集新工艺

付小佼，储满生，高立华，柳政根

东北大学 冶金学院，沈阳 110819

摘　要：实现低品位硼镁铁共生矿的综合利用，提出新的清洁生产工艺路线，通过金属化还原−磁选分离、硫酸浸出和浸出液加入乙醇结晶，提取其中的镁资源，可分别得到富铁产品、富硅产品和富硼产品。金属化还原−磁选环节中，在还原温度 1250 ℃、还原时间 60 min、矿粒度 0.50~2.00 mm 和煤粒度 0.50~1.50 mm 条件下，原矿中94.6%的镁可富集到非磁性产物中。非磁性产物在浸出温度 90 ℃、浸出时间 15 min 和液固比 7:1 的条件下和硫酸反应，87.4%的镁可富集到溶液中，从而与残留在浸出渣中的硅分离。镁离子浓度为 0.8 mol/L 的浸出液常温下加入原始溶液体积 1.5 倍的乙醇静置 30 min 后，97.2%的镁以 $MgSO_4 \cdot 7H_2O$ 的形式结晶析出。

关键词：硼镁铁共生矿；镁；金属化还原；浸出；结晶；回收

(Edited by Xiang-qun LI)